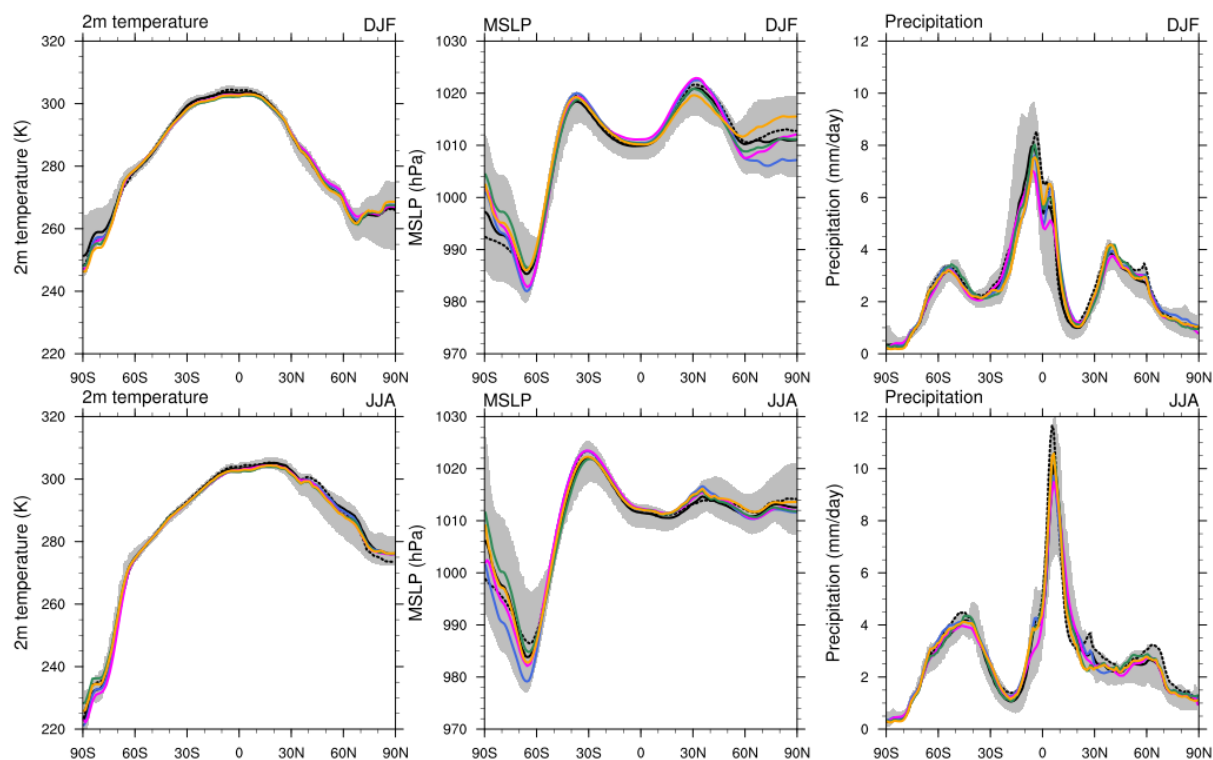# Supplementary material

Figure S1. Seasonal means of zonal mean of 2m temperature (left), mean sea level pressure (middle), and precipitation (right), in the SSP585 simulations and in the CMIP6 scenario SSP5 8.5 simulations (years 2080 - 2099). The blue (CESM2), magenta (NorESM2), green (EC-Earth3) and yellow (OpenIFS) lines show the models applied in the present study and the black line shows the CMIP6 multi-model mean and black dashed line shows ACCESS-ESM1.5 CMIP6 simulation where sea ice cover and SST were taken. The gray area shows the range between the minimum and maximum of the 23 CMIP6 models. The upper row shows mean values for northern hemisphere winter (DJF) and the lower row shows mean values for southern hemisphere winter (JJA).
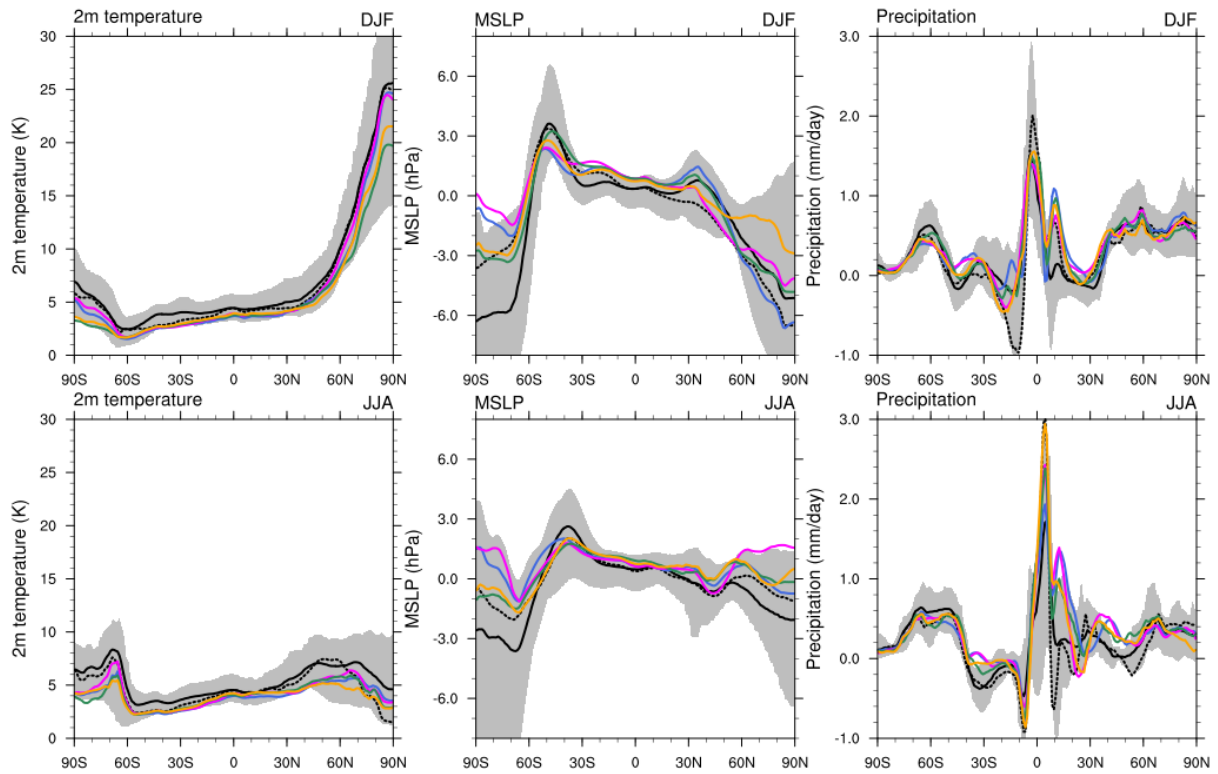
Figure S2. Seasonal mean differences of zonal mean of 2m temperature (left), mean sea level pressure (middle), and precipitation (right), between the SSP585 and baseline simulations and in the CMIP6 scenario SSP5 8.5 and historical simulations (2080 - 2099). The blue (CESM2), magenta (NorESM2), green (EC-Earth3) and yellow (OpenIFS) lines show the models applied in the present study and the black line shows the CMIP6 multi-model mean and black dashed line shows ACCESS-ESM1.5 CMIP6 simulation where sea ice cover and SST were taken. The gray area shows the range between the minimum and maximum of the 23 CMIP6 models. The upper row shows mean values for northern hemisphere winter (DJF) and the lower row shows mean values for southern hemisphere winter (JJA).
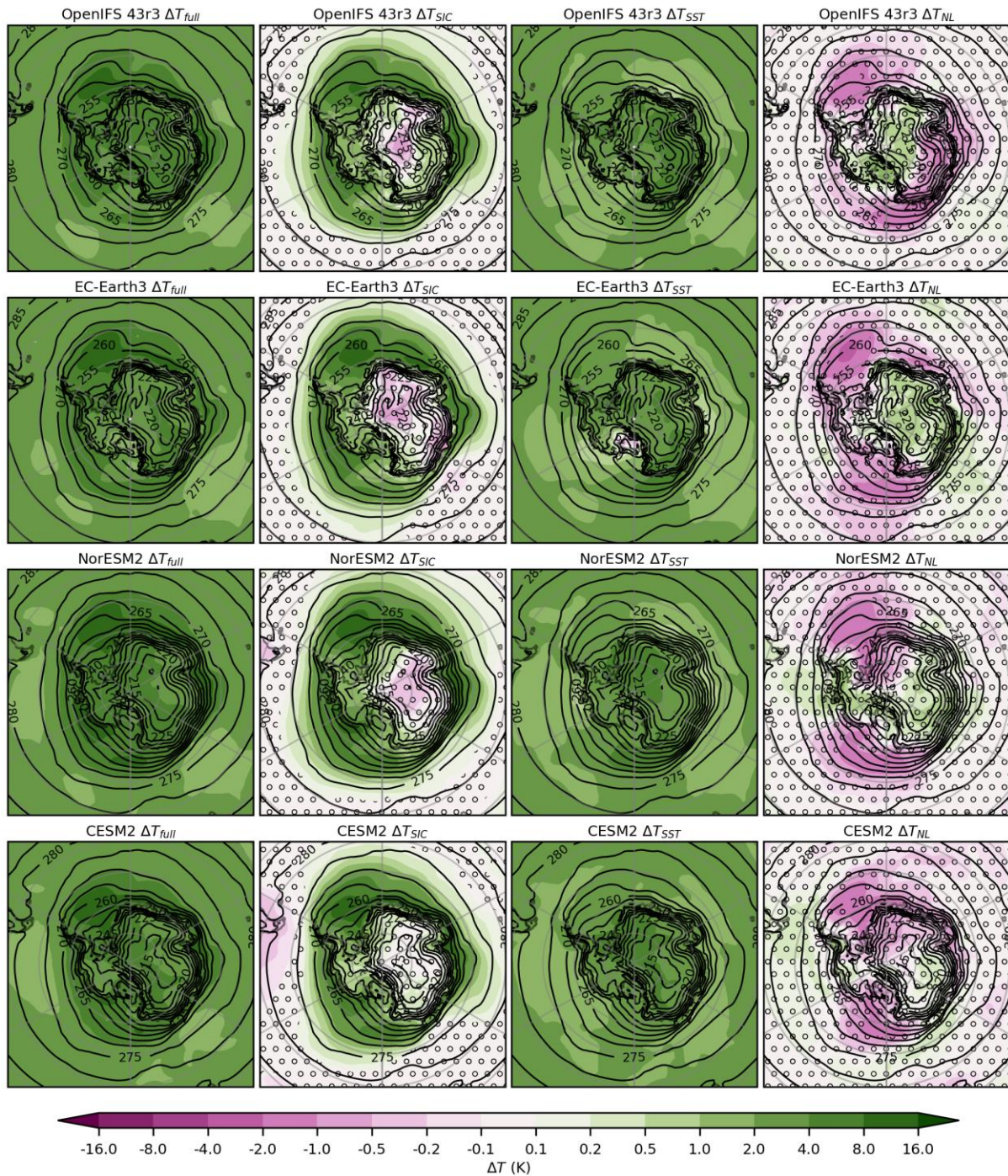
Figure S3. Difference in 2m temperature (T) in southern hemisphere winter (JJA) between the SSP585 simulation and Baseline (ΔT_{full},left), between SIC_SSP585 and Baseline (ΔT_{SIC},2nd left), between SST_SSP585 and Baseline (ΔT_{SST},3rd left) and the nonlinear (ΔT_{NL} residual) contribution (right). The model in the 1st row is OpenIFS, 2nd row is EC-Earth3, 3rd row is NorESM2 and 4th row is CESM2. Stippling indicates that the changes are not statistically significant based on t-test with p-value 0.05.
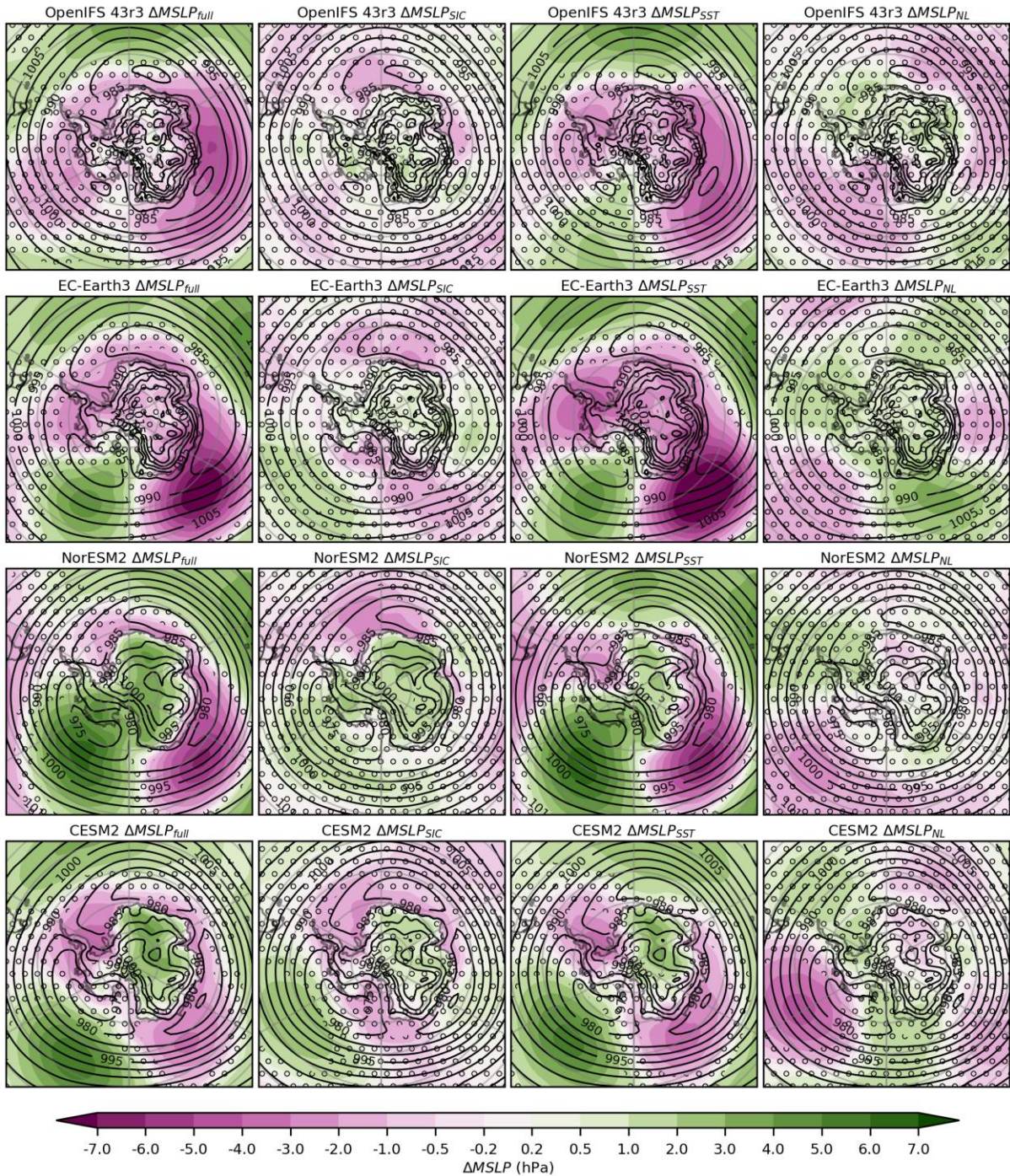
Figure S4. Difference in mean sea level pressure (MSLP) in southern hemisphere winter (JJA) between the SSP585 simulation and Baseline (ΔT_{full},left), between SIC_SSP585 and Baseline (ΔT_{SIC},2nd left), between SST_SSP585 and Baseline (ΔT_{SST},3rd left) and the nonlinear (ΔT_{NL} residual) contribution (right). The model in the 1st row is OpenIFS, 2nd row is EC-Earth3, 3rd row is NorESM2 and 4th row is CESM2. Stippling indicates that the changes are not statistically significant based on t-test with p-value 0.05.
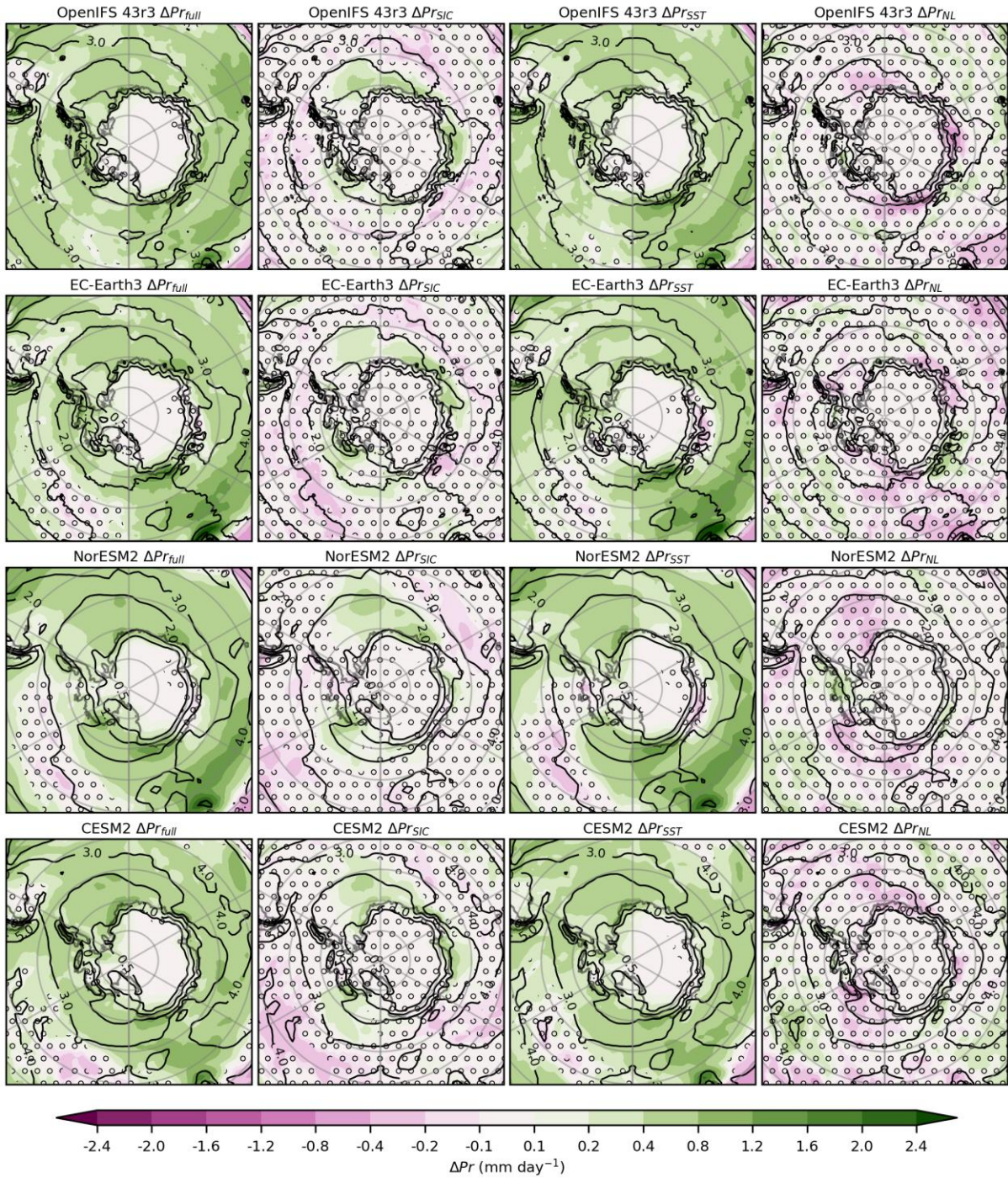
Figure S5. Difference in precipitation (Pr) in southern hemisphere winter (JJA) between the SSP585 simulation and Baseline (ΔT_{full}, left), between SIC_SSP585 and Baseline (ΔT_{SIC}, 2nd left), between SST_SSP585 and Baseline (ΔT_{SST}, 3rd left) and the nonlinear (ΔT_{NL}, residual) contribution (right). The model in the 1st row is OpenIFS, 2nd row is EC-Earth3, 3rd row is NorESM2 and 4th row is CESM2. Stippling indicates that the changes are not statistically significant based on t-test with p-value 0.05.
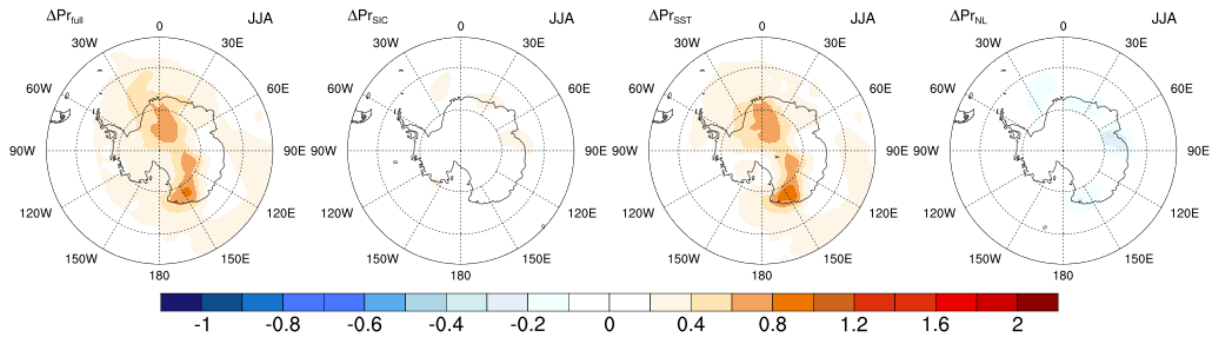
Figure S6. Multi-model mean relative difference in precipitation (Pr) in northern hemisphere winter (JJA) between the SSP585 simulation and Baseline (ΔT_{full},left), between SIC_SSP585 and Baseline (ΔT_{SIC},2nd left), between SST_SSP585 and Baseline (ΔT_{SST},3rd left) and the nonlinear (ΔT_{NL} residual) contribution (right).
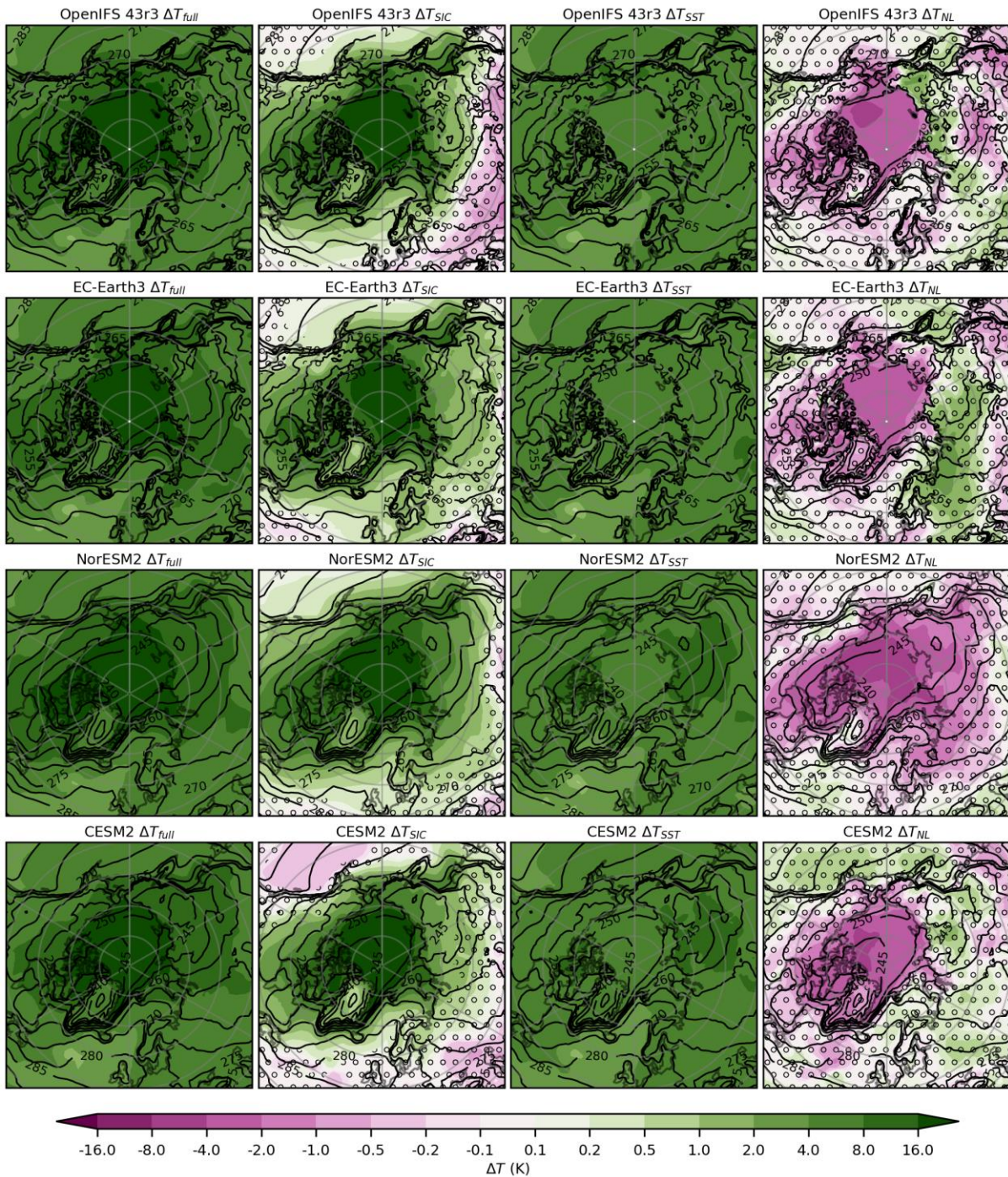
Figure S7. Difference in 2m temperature (T) in northern hemisphere winter (DJF) between the SSP585 simulation and Baseline (ΔT_full, left), between SIC_SSP585 and Baseline (ΔT_SIC, 2nd left), between SST_SSP585 and Baseline (ΔT_SST, 3rd left) and the nonlinear (ΔT_NL residual) contribution (right). The model in the 1st row is OpenIFS, 2nd row is EC-Earth3, 3rd row is NorESM2 and 4th row is CESM2. Stippling indicates that the changes are not statistically significant based on t-test with p-value 0.05.
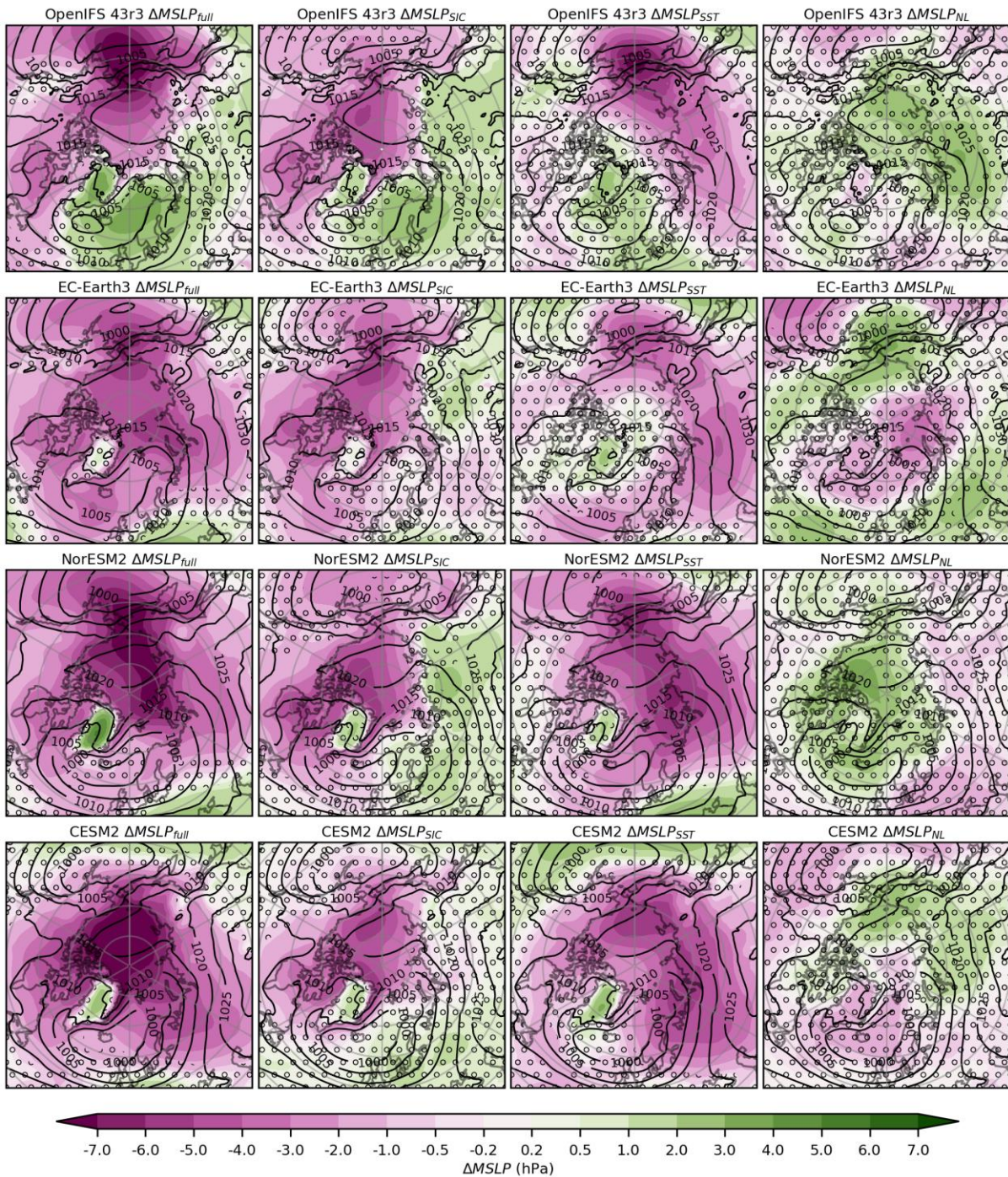
Figure S8. Difference in mean sea level pressure (MSLP) in northern hemisphere winter (DJF) between the SSP585 simulation and Baseline ($\Delta MSLP_{full}$, left), between SIC_SSP585 and Baseline ($\Delta MSLP_{SIC}$, 2nd left), between SST_SSP585 and Baseline ($\Delta MSLP_{SST}$, 3rd left) and the nonlinear ($\Delta MSLP_{NL}$ residual) contribution (right). The model in the 1st row is OpenIFS, 2nd row is EC-Earth3, 3rd row is NorESM2 and 4th row is CESM2. Stippling indicates that the changes are not statistically significant based on t-test with p-value 0.05.
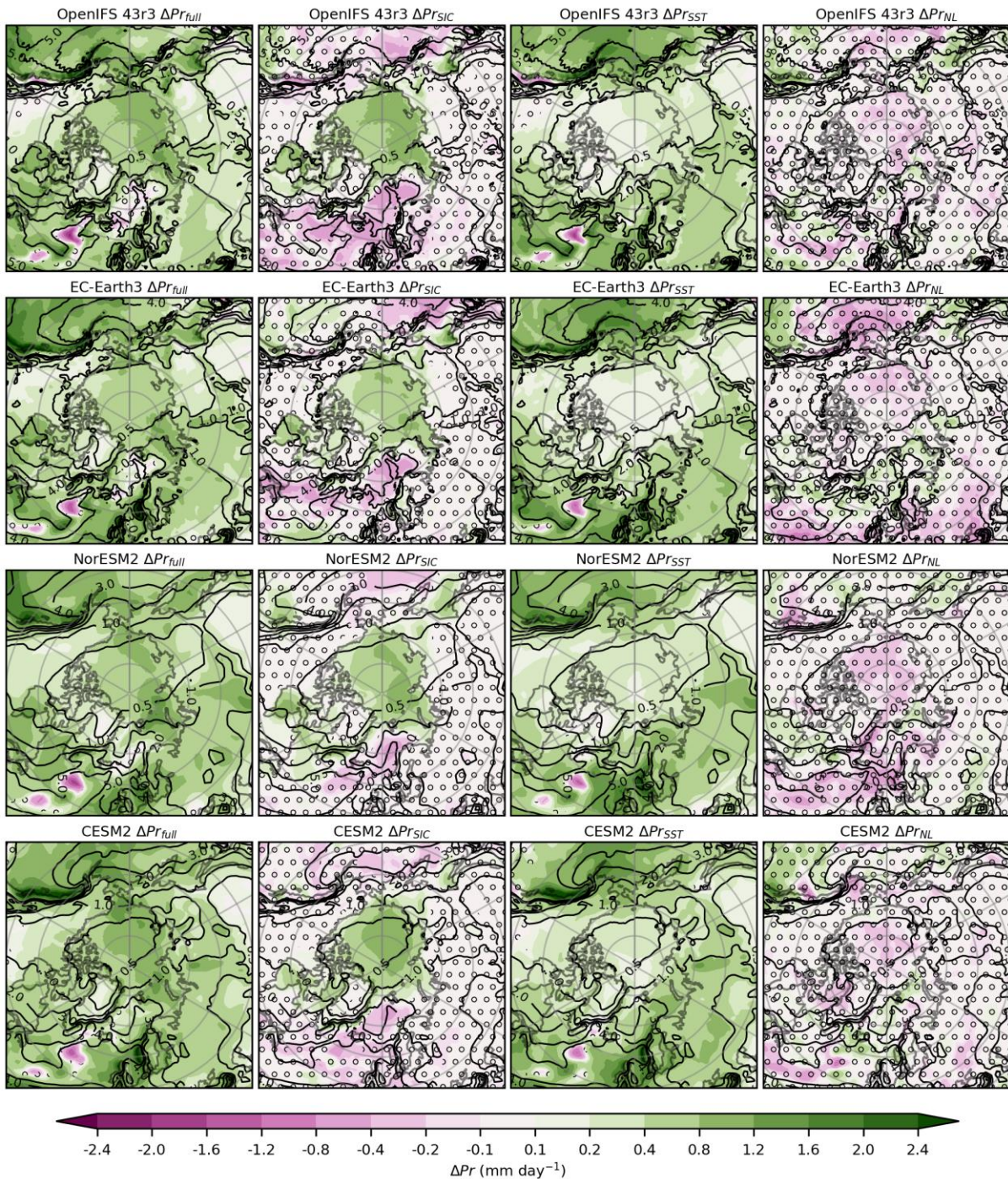
Figure S9. Difference in precipitation (Pr) in northern hemisphere winter (DJF) between the SSP585 simulation and Baseline (ΔPr_{full}, left), between SIC_SSP585 and Baseline (ΔPr_{SIC}, 2nd left), between SST_SSP585 and Baseline (ΔPr_{SST}, 3rd left) and the nonlinear (ΔPr_{NL} residual) contribution (right). The model in the 1st row is OpenIFS, 2nd row is EC-Earth3, 3rd row is NorESM2 and 4th row is CESM2. Stippling indicates that the changes are not statistically significant based on t-test with p-value 0.05.
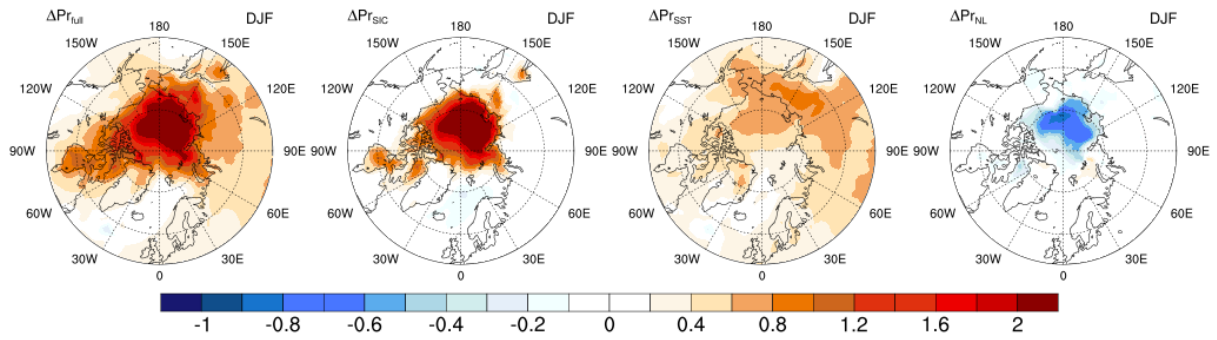
Figure S10. Relative difference in precipitation (Pr) in northern hemisphere winter (DJF) between the SSP585 simulation and Baseline (ΔPr_{full}, left), between SIC_SSP585 and Baseline (ΔPr_{SIC}, 2nd left), between SST_SSP585 and Baseline (ΔPr_{SST}, 3rd left) and the nonlinear (ΔPr_{NL} residual) contribution (right). The model in the 1st row is OpenIFS, 2nd row is EC-Earth3, 3rd row is NorESM2 and 4th row is CESM2 shows the multi-model mean and the lower row the maximum difference between models. Stippling indicates that the changes are not statistically significant.
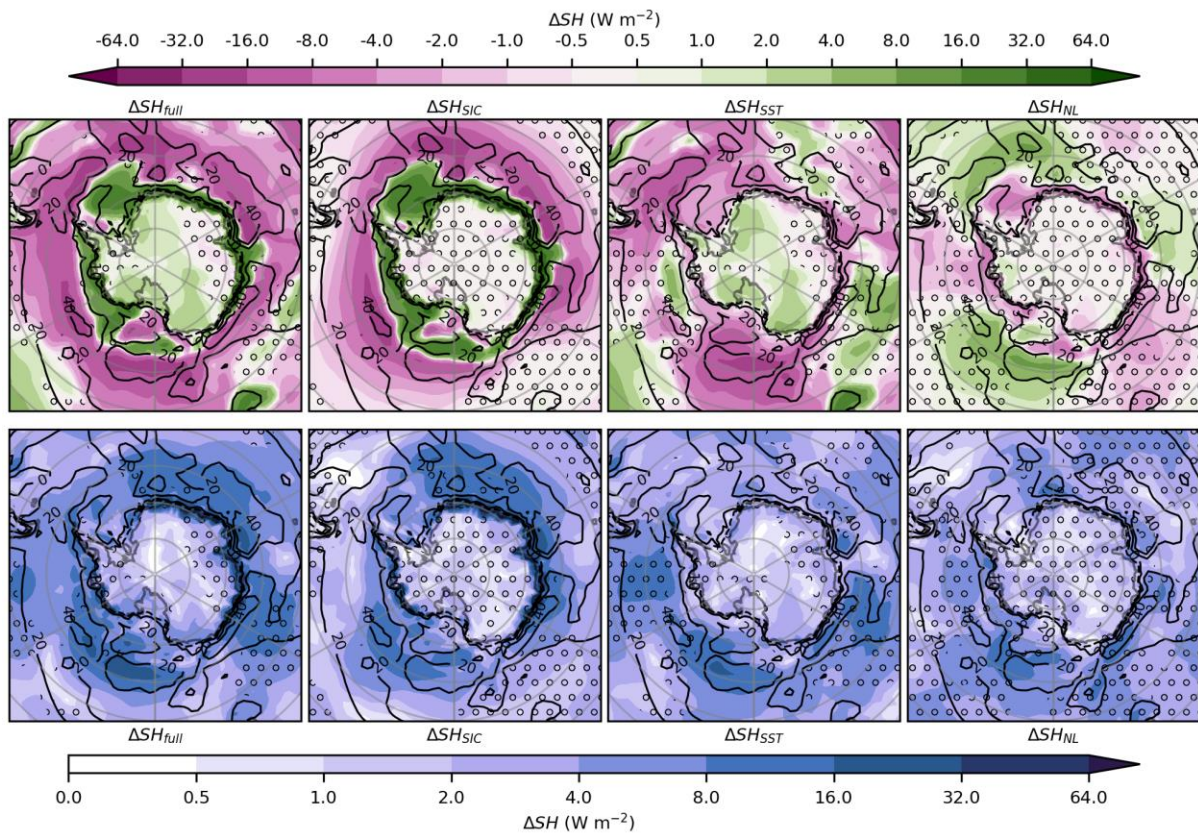
Figure S11. Difference in sensible heat flux (SH) in southern hemisphere winter (JJA) between the SSP585 simulation and Baseline (ΔSH_{full}, left), between SIC_SSP585 and Baseline (ΔSH_{SIC}, 2nd left), between SST_SSP585 and Baseline (ΔSH_{SST}, 3rd left) and the nonlinear (ΔSH_{NL} residual) contribution (right). The upper row shows the multi-model mean and the lower row the maximum difference between models. Stippling indicates that all models do not agree on the direction of the change.
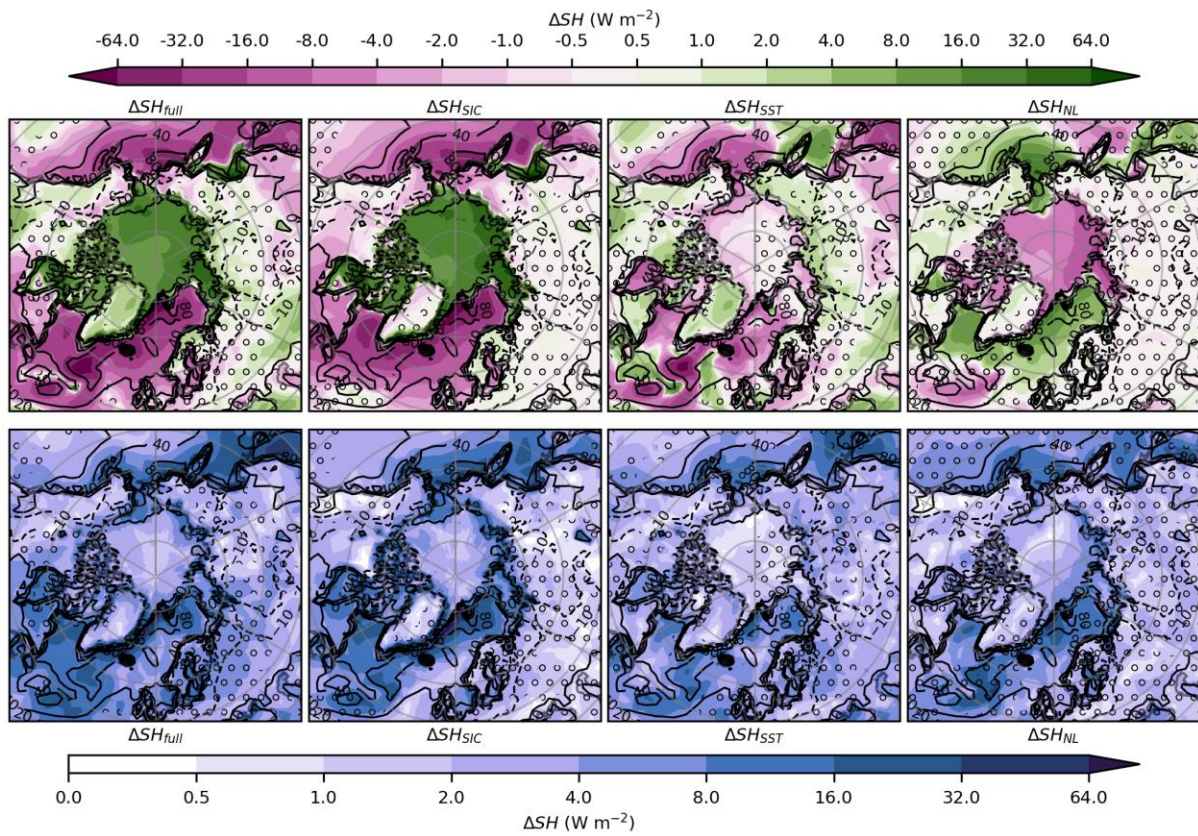
Figure S12. Difference in sensible heat flux (SH) in northern hemisphere winter (DJF) between the SSP585 simulation and Baseline (ΔSH_{full},left), between SIC_SSP585 and Baseline (ΔSH_{SIC},2nd left), between SST_SSP585 and Baseline (ΔSH_{SST},3rd left) and the nonlinear (ΔSH_{NL} residual) contribution (right). The upper row shows the multi-model mean and the lower row the maximum difference between models. Stippling indicates that all models do not agree on the direction of the change.
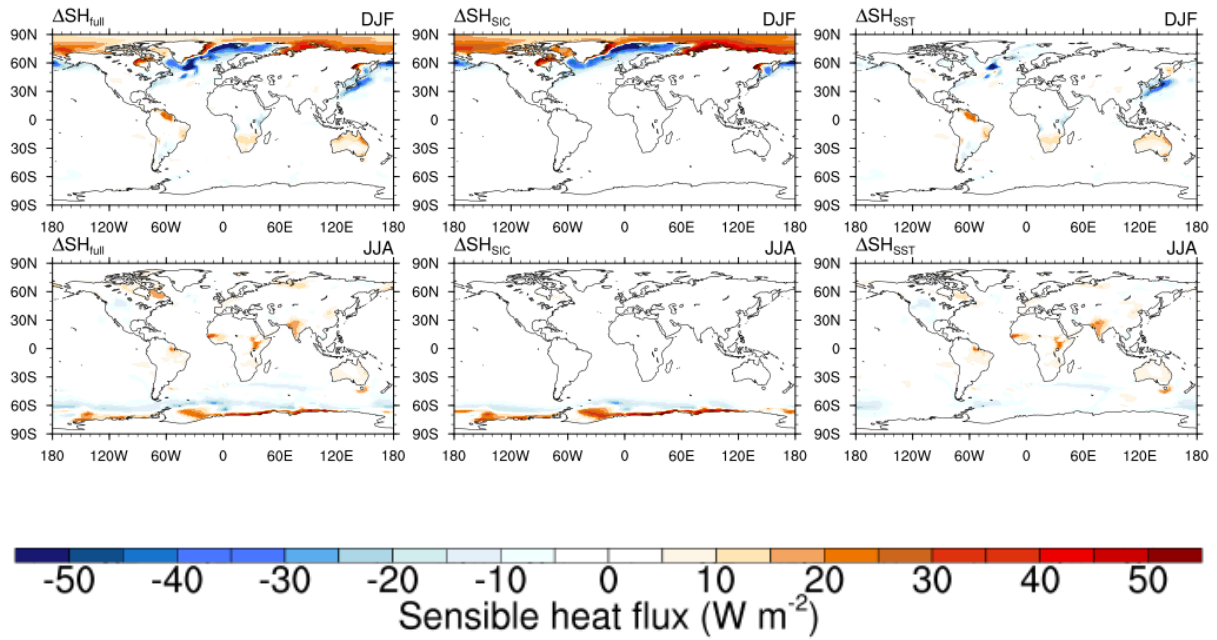
Figure S13. Difference in sensible heat flux (SH) in southern hemisphere winter (JJA, upper row) and in northern hemisphere winter (DJF, lower row) between the SSP585 simulation and Baseline (ΔSH_{full}, left), between SIC_SSP585 and Baseline (ΔSH_{SIC}, middle), between SST_SSP585 and Baseline (ΔSH_{SST}, right).
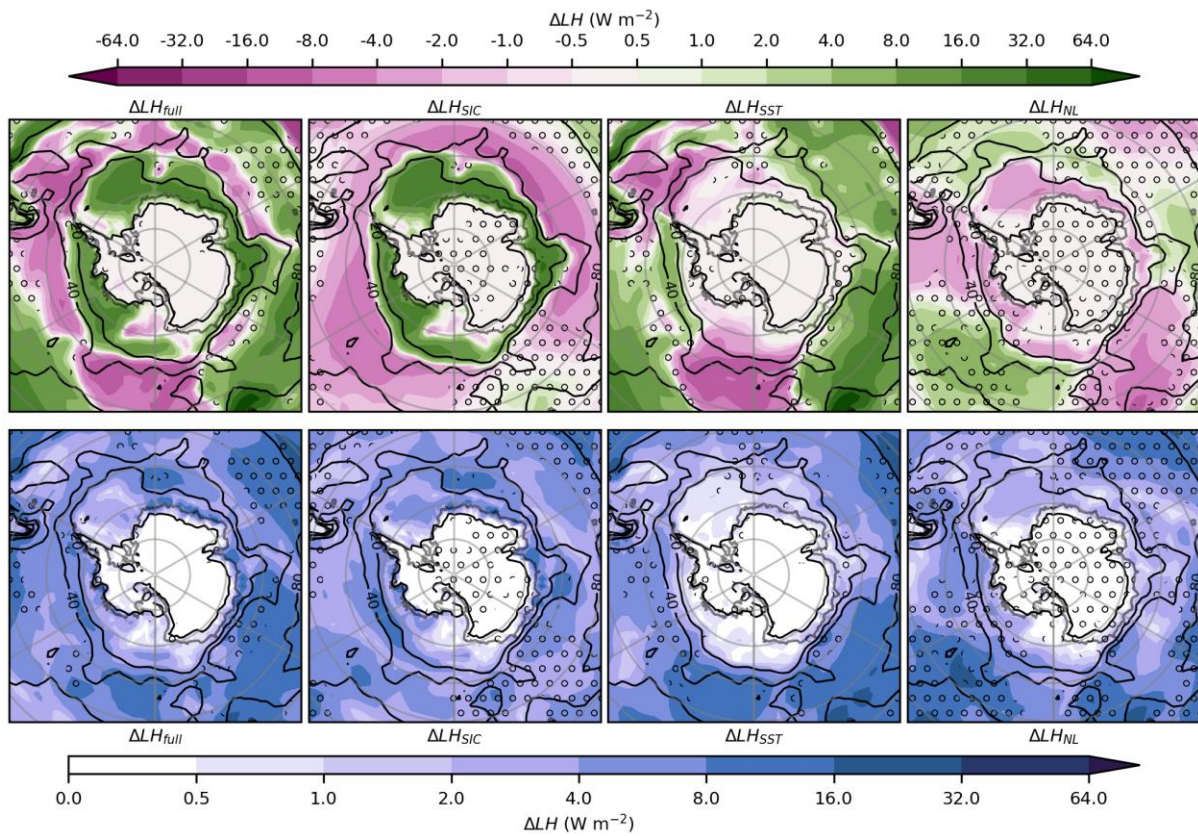
Figure S14. Difference in latent heat flux (LH) in southern hemisphere winter (JJA) between the SSP585 simulation and Baseline (ΔLH_{full},left), between SIC_SSP585 and Baseline (ΔLH_{SIC},2nd left), between SST_SSP585 and Baseline (ΔLH_{SST},3rd left) and the nonlinear (ΔLH_{NL} residual) contribution (right). The upper row shows the multi-model mean and the lower row the maximum difference between models. Stippling indicates that all models do not agree on the direction of the change.
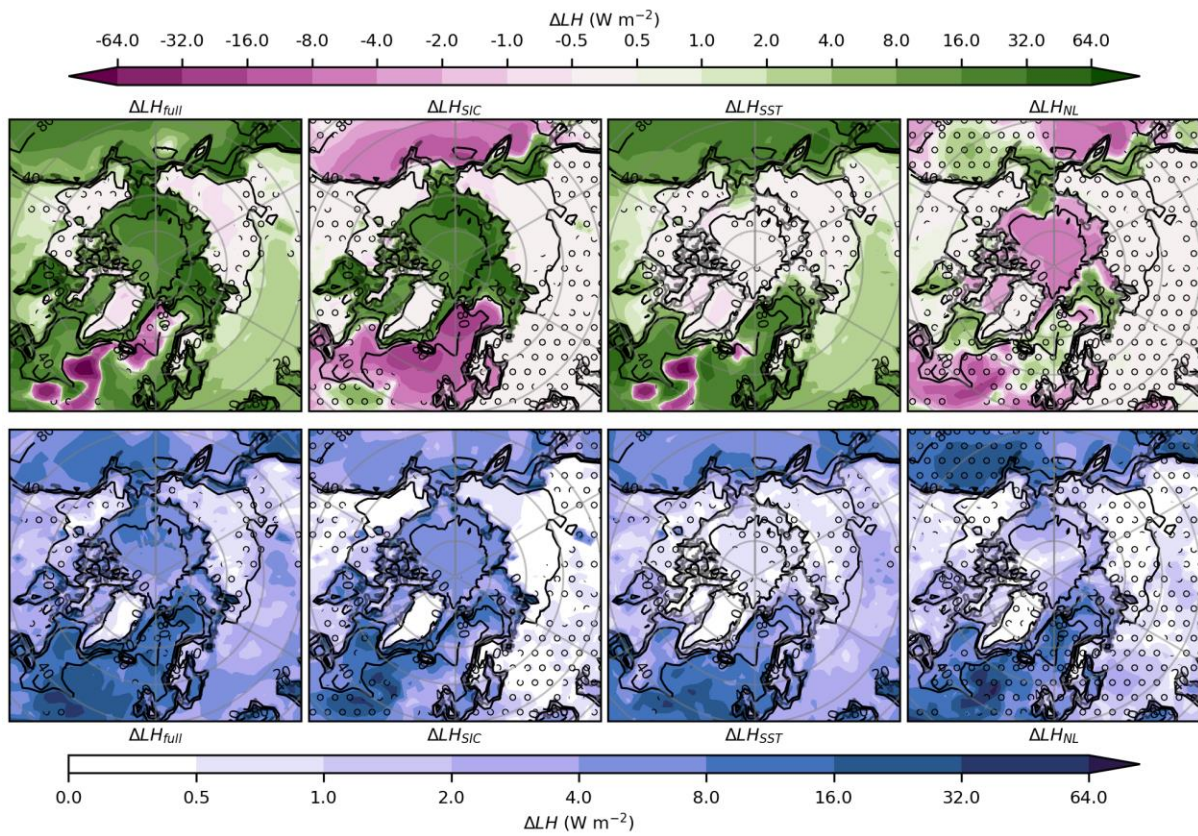
Figure S15. Difference in latent heat flux (LH) in northern hemisphere winter (DJF) between the SSP585 simulation and Baseline (ΔLH_{full}, left), between SIC_SSP585 and Baseline (ΔLH_{SIC}, 2nd left), between SST_SSP585 and Baseline (ΔLH_{SST}, 3rd left) and the nonlinear ($\Delta LHNL$ residual) contribution (right). The upper row shows the multi-model mean and the lower row the maximum difference between models. Stippling indicates that all models do not agree on the direction of the change.
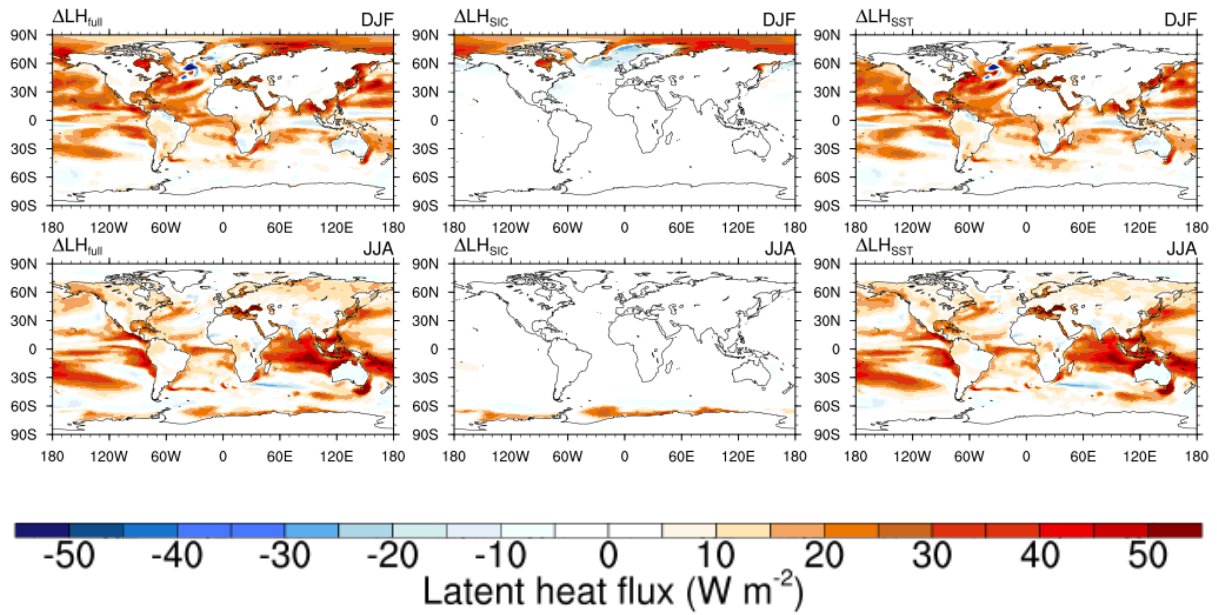
Figure S16. Difference in latent heat flux (LH) in southern hemisphere winter (JJA, upper row) and in northern hemisphere winter (DJF, lower row) between the SSP585 simulation and Baseline (ΔLH$_{full}$,left), between SIC_SSP585 and Baseline (ΔLH$_{SIC}$,2nd left), between SST_SSP585 and Baseline (ΔLH$_{SST}$,3rd left).
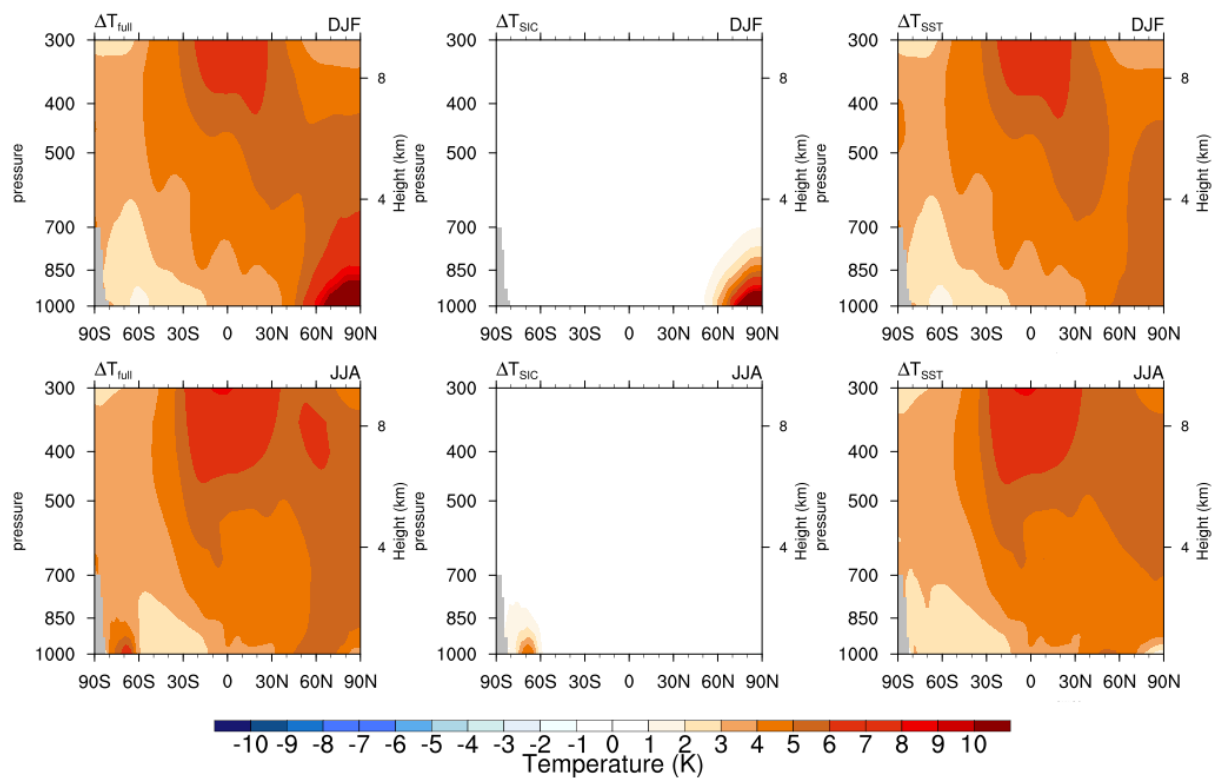
Figure S17. Zonal-mean temperature difference in northern hemisphere winter (DJF, upper row) and in southern hemisphere winter (JJA, lower row) between the SSP585 simulation and Baseline (ΔT$_{full}$, left), between SIC_SSP585 and Baseline (ΔT$_{SIC}$, middle), between SST_SSP585 and Baseline (ΔT$_{SST}$, right).
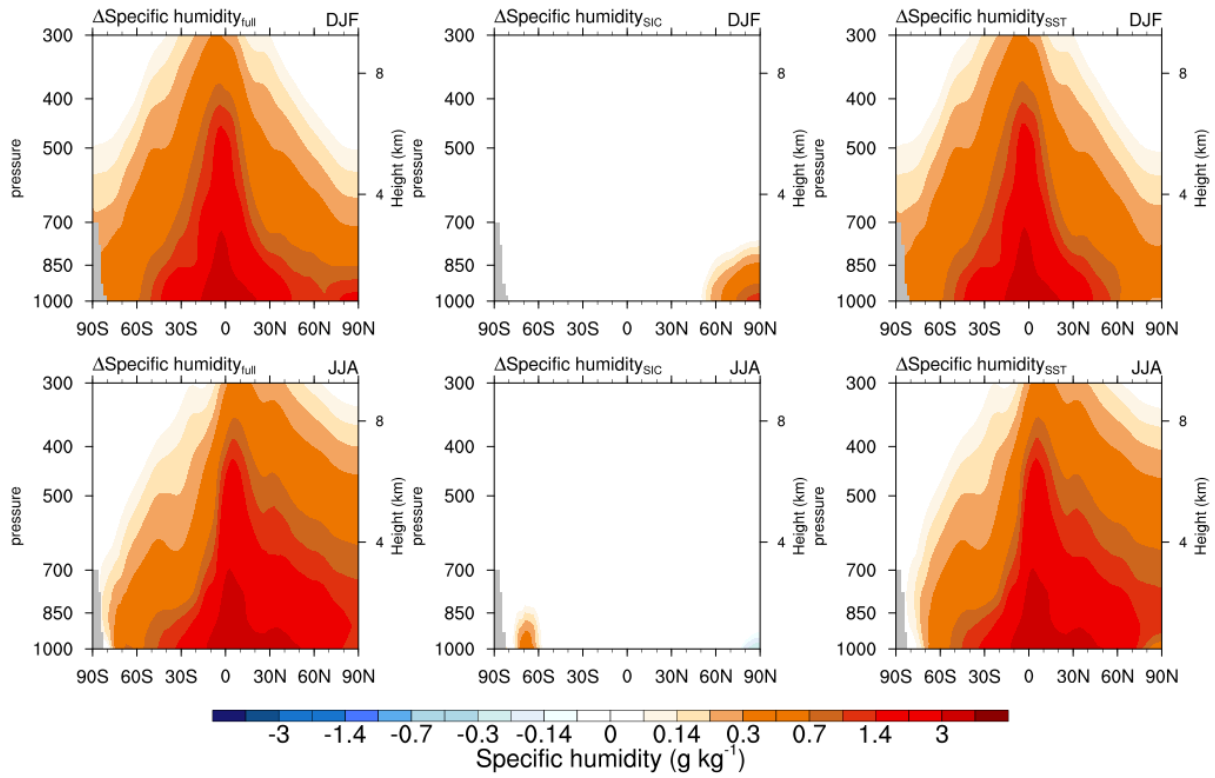
Figure S18. Zonal-mean specific humidity difference (g / kg) in northern hemisphere winter (DJF, upper row) and in southern hemisphere winter (JJA, lower row) between the SSP585 simulation and Baseline (Δq_{FULL}, left), between SIC_SSP585 and Baseline (Δq_{SIC}, middle), between SST_SSP585 and Baseline (Δq_{SST}, right).